RSC Advances

PAPER

View Article Online
View Journal | View Issue

Cite this: *RSC Adv.*, 2017, **7**, 45818

Evolution of the formation of a covalent triazine-based framework catalyzed by *p*-toluenesulfonic acid monohydrate†

Zheng Li,[ab] Yue Han,[d] Ying Guo,[a] Shuangshuang Xu,[c] Fenghua Chen,[a] Li Ye,[a] Zhenhua Luo,[a] Xiang Liu,[a] Heng Zhou*[ab] and Tong Zhao *[ab]

A porous covalent triazine-based framework (CTF) was prepared by a two-step strategy, where *p*-toluenesulfonic acid monohydrate ($TsOH \cdot H_2O$) was used as a catalyst. The porosity and gas storage capacity of the as-obtained framework was evaluated. In addition, the evolution of the chemical structure during the two stages was studied. Crystallite size was calculated to study the formation of the framework; the evolution of internal porosity has been discussed based on the results obtained. In the first step, a triazine-based polymer was formed at relatively low temperatures, and limited crystallites were developed. However, in the second step, a treatment at higher temperatures performed in an open system resulted in the purification of the chemical structure; furthermore, CTF lamellae with an improved ordered stacking developed, resulting in a dramatic increase in internal porosity.

Received 28th June 2017
Accepted 12th September 2017

DOI: 10.1039/c7ra07181g

rsc.li/rsc-advances

Introduction

Porous materials, possessing a large amount of small pores and thus high surface areas, can be used in various fields such as in catalysis (catalysts or catalyst supports),[1,2] adsorption, separation,[3,4] gas storage,[5] and ion exchange.[6] In particular, organic porous materials have attracted significant attention due to their lightweight properties, flexible design, and ease of functionalization.[7–9] Over the last few years, purely organic materials with small pores, such as hyper-crosslinked polymers, polymers with intrinsic microporosity, and covalent organic frameworks (COFs), have been reported.[10–16] Among these, COFs, a kind of microporous, crystalline polymer networks with periodic pore structures, have attracted increasing attention in recent years. Their tunable pore size and tailored functionalities indicate that COFs can find potential applications in a diverse range of fields, such as optoelectronics, electrochemistry, and catalysis.[17–20] The first COF, COF-1, synthesized *via* reversible formation of a boronate ester, exhibited a high surface area and good thermal stability.[21] Other COFs were synthesized *via* formation of boronate anhydrides, borosilicates, imines, hydrazones, and triazines.[22]

CTFs are an emerging type of partially crystalline porous frameworks that possess properties similar to those of COFs.[23] Being isoelectronic to COF-1, CTF-1s polymerize from DCB and possess comparable porous properties, whereas the triazine structures provide better thermal and chemical stability than the boroxine rings. It has been reported that CTFs can be used as catalyst supports for selective reactions at high temperatures, solid phase catalysts for the conversion of CO_2, and carriers or sorbent materials for storing gases.[24–26] Moreover, CTFs have been recently applied as sensors and electrodes.[27] CTFs can be synthesized by trimerization reaction of carbonitriles, such as the relatively easier accessible monomer 1,4-dicyanobenzene (DCB), using $ZnCl_2$ as a Lewis acid[28–30] to obtain a so-called ionothermal system;[31] however, due to the weak acidity and high melting point of $ZnCl_2$, high initial reaction temperatures and large catalyst dosages are necessary when $ZnCl_2$ is used as a catalyst. Other potential catalysts are organic acids. As reported, the most widely used organic acid is trifluoromethanesulfonic acid (CF_3SO_3H), a strong Brønsted acid with a very high volatility.[32–34] The relationship between catalyst dosage and the Brunauer–Emmett–Teller specific surface area (BET SSA) of reported CTF-1s is illustrated in Fig. 1 for better comparison.[23,32–34]

In this study, *p*-toluenesulfonic acid monohydrate ($TsOH \cdot H_2O$), a solid-state organic acid with medium-strong acidity, was selected as the catalyst for the synthesis of CTF-1. The evolution of the CTF framework construction, along with the pore formation, was elucidated by chemical structure analysis and crystal parameter calculations. In addition,

[a]*Laboratory of Advanced Polymer Material, Institute of Chemistry, Chinese Academy of Sciences, Beijing 100190, China. E-mail: tzhao@iccas.ac.cn; zhouheng@iccas.ac.cn; Fax: +86-10-62562750; Tel: +86-10-62562750*

[b]*University of Chinese Academy of Sciences, Beijing 100049, China*

[c]*School of Material Science and Engineering, Beihang University, Beijing 100191, China*

[d]*South China Advanced Institute for Soft Matter Science and Technology, South China University of Technology, 510640 Guangzhou, PR China*

† Electronic supplementary information (ESI) available. See DOI: 10.1039/c7ra07181g

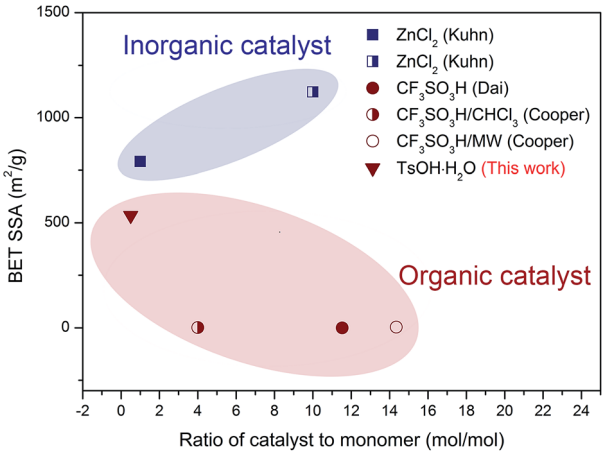

Fig. 1 Comparison of the catalyst to monomer ratio and the BET SSA of various CTF-1s catalyzed by different catalysts (data was derived from the corresponding literature).[23,28–30]

a method for crystallite size calculation was developed based on the deconvoluted powder X-ray diffractometer (PXRD) patterns, which shows great potential in demonstrating the relationship between the crystallite development and porosity formation.

Experimental

Chemicals

DCB was obtained from J&K Scientific Ltd. TsOH·H_2O was purchased from Sinopharm Chemical Reagent Beijing Co. Ltd. All chemicals were used as received.

Synthesis of the triazine-based polymer

DCB (1.28 g, 10 mmol) and TsOH·H_2O (0.95 g, 5 mmol) were mixed using a mortar and transferred to a quartz ampoule (3 × 7 cm) under a nitrogen atmosphere. The ampoule was vacuumed, sealed, and heated at 250 °C for 5 h, then at 300 °C for 5 h, and finally at 350 °C for 10 h. Subsequently, the ampoule was allowed to cool down to room temperature and then opened. The as-obtained triazine-based polymer was solid and black in colour.

Post-processing of the triazine-based polymer

The triazine-based polymer (0.42 g) was added to a porcelain crucible, covered with a lid, and placed inside a quartz tubular furnace. No further catalyst was added to the system during this process. Then, under a nitrogen atmosphere, the crucible was heated to either 400 °C or 500 °C, and this temperature was maintained for 20 h. Both as-obtained solid products were black in color and were designated as CTF-1@400 (prepared at 400 °C) and CTF-1@500 (prepared at 500 °C).

Characterizations

Fourier transform infrared spectroscopy (FTIR) spectra were obtained using a Tensor-27 spectrometer at room temperature. X-ray photoelectron spectroscopy (XPS) measurements were performed using an ESCALAB250XI instrument. ^{13}C-solid-state nuclear magnetic resonance (^{13}C-solid NMR) spectra were obtained using a Bruker Avance 400 MHz spectrometer. Powder X-ray diffractograms (PXRD) were obtained in the reflection mode using a Rigaku D/max 2500 powder X-ray diffractometer with Cu-K_α radiation (λ = 1.4518 Å). Nitrogen sorption measurements were performed at 77 K using a Micromeritics ASAP 2020 surface area and porosimetry analyzer. Pyrolysis-gas chromatography/mass spectrometry (Py-GC/MS) experiments were performed using a EGA/PY-303D pyrolyser connected to a QP2010Ultra GC-MS. Finally, elemental analysis was performed using a Flash EA 1112 analyzer.

Calculation of the crystallite size

PXRD patterns were baseline corrected and smoothed using the MDI Jade software, and the deconvolution of the curves was performed using the Origin software. The *d*-spacing (d_{hkl}) and the crystallite dimension (D_{hkl}) were calculated by the following equations:

The Bragg equation:

$$d_{hkl} = \frac{n\lambda}{2 \sin \theta}, \quad (1)$$

where n is the diffraction series (herein, it was adopted as 1), θ is the Bragg diffraction angle, and λ is the X-ray wavelength (Cu K_α, 1.5418 Å).

The Scherrer equation:

$$D_{hkl} = \frac{K\lambda}{\beta \times \cos \theta}, \quad (2)$$

where K is the crystallite shape constant (herein, it was adopted as 0.89), and β is the crystallite size-induced diffraction width. According to its definition, β equals to the full width at half maximum of the corresponding diffraction peak in the PXRD pattern.[35]

Results and discussion

Characterization of the CTF structures

The chemical structure of CTF-1@500 was confirmed by FTIR, XPS and ^{13}C solid NMR. In the FTIR spectrum of CTF-1@500 (Fig. 2a), the absence of the peak corresponding to the nitrile group (2230 cm^{-1}) and the presence of clear peaks for triazine structures (1515 and 1350 cm^{-1}) indicated the successful transformation of the nitrile groups into triazine structures *via* trimerization. The structure of CTF-1@500 was also confirmed by XPS. The peak with a binding energy of 286.8 eV (corresponding to triazine carbon) in the deconvoluted C 1s spectrum (Fig. 2f) and the peak at a binding energy of 398.9 eV (corresponding to triazine N 1s signal) in the N 1s spectrum (Fig. 2g) were in agreement with the FTIR results.[4] In addition, the peak at 169.8 ppm in the ^{13}C solid NMR of CTF-1@500 (Fig. S1†), attributing to the triazine structure, further verified the existence of triazine structure in CTF-1@500.

The periodic chemical structure of CTF-1@500 was calculated using the Materials Studio software (Fig. 2c). The structure of the crystal cell is shown in Fig. S2,† from which the PXRD

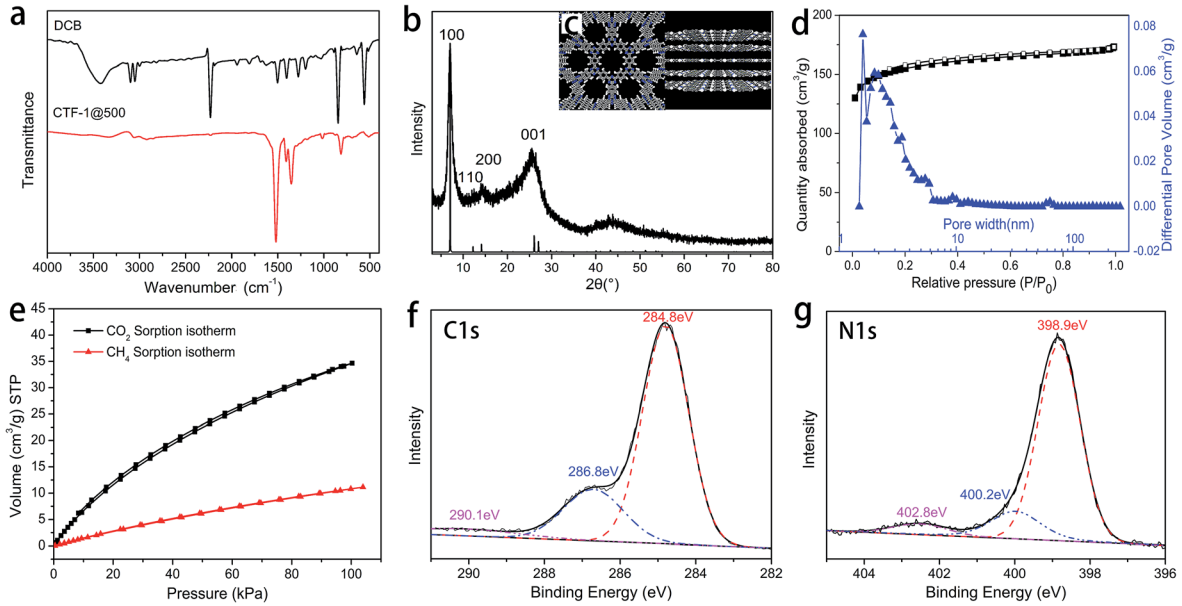

Fig. 2 (a) FTIR spectra of DCB and CTF-1@500; (b) experimental PXRD pattern of CTF-1@500 (top) and calculated PXRD pattern based on an optimized CTF-1 structure; (c) CTF-1 structure as calculated using the Materials Studio software; (d) nitrogen adsorption–desorption isotherms (black) and pore size distribution (blue) of CTF-1@500; (e) volumetric CO_2 (black) and CH_4 (red) sorption isotherms of CTF-1@500 at 298 K; (f) deconvoluted C 1s spectrum of CTF-1@500; and (g) deconvoluted N 1s spectrum of CTF-1@500.

pattern is predicted and shown in Fig. 2b. Obviously, the observed PXRD signals appear at almost the same positions as the calculated value; thus, the formation of crystalline triazine-based frameworks is confirmed.

The hexagonally packed triazine-based framework would bring in large quantity of nanopores, and the pore structure of CTF-1@500 was investigated by nitrogen sorption experiments at 77 K. The type I isotherm (Fig. 2d) indicated the presence of abundant micropores, and the BET SSA was determined to be 535 $m^2 g^{-1}$. As illustrated in Fig. 1, using $TsOH \cdot H_2O$, an organic acid with medium acidity, a smaller amount of catalyst was needed and a higher BET SSA was achieved, as compared to that of CTF-1 prepared with CF_3SO_3H. The maximum value for the pore size as calculated by the non-local density functional theory (NL-DFT) was 15.91 Å, which was quite close to the unit cell parameter ($a = b = 12.58$ Å, Fig. S2†). Moreover, the adsorption capacity of CTF-1@500 for CO_2 and CH_4 at 298 K were measured to evaluate their potential application as gas capture and storage materials. The volumetric CO_2 and CH_4 sorption isotherms (Fig. 2e) show that the uptakes at 1 bar for CO_2 and CH_4 are 1.5 mmol g^{-1} and 0.50 mmol g^{-1}, respectively. The result indicates remarkable capacity of CTF-1@500 for gas, especially for CO_2. This capacity was relatively higher than that of CTF-1 prepared with $ZnCl_2$ (ref. 4) (1.41 mmol g^{-1}).

Evolution during pore formation

Under acidic conditions, nitriles tend to transform into triazine structures *via* trimerization. Polymerization of DCB catalyzed by TsOH was carried out below a relatively low temperature (350 °C) in a vacuum-sealed system. The reaction for the catalytic trimerization of DCB is shown in Scheme 1a. The protons of TsOH could facilitate the nucleophilic addition of nitrile groups; this formed the triazine-based polymer. Subsequently, during the treatment at 500 °C in an open system, the ongoing reversible trimerization reaction would benefit the growth of CTF crystals into larger and thicker lamellae to afford CTF-1@500. However, due to the existence of both steric and kinetic limitations, the final CTF solid at equilibrium consisted of a combination of crystalline and amorphous domains, as illustrated in Scheme 1b.

To study the evolution of the framework construction, CTF-1@400 was prepared from the triazine-based polymer *via* a similar post treatment at 400 °C as CTF-1@500. Chemical and structural characterizations were performed on the products obtained at the first stage (triazine-based polymer) and at the second stage (CTF-1@400 and CTF-1@500) to reveal the evolution.

The FTIR spectra (Fig. 3a) indicated that early in the first step (polymerization), triazine structures (1515 and 1350 cm^{-1}) are formed; after the post-treatment, CTF-1@400 and CTF-1@500 largely retain such structure. In the XPS results, the signals at 286.8 eV in the deconvoluted C 1s spectra and 398.9 eV in the deconvoluted N 1s spectra (Fig. S3†) further verify the successful formation and retention of triazine rings in triazine-based polymer, CTF-1@400 and CTF-1@500. The disappearance of the weak peak at around 1720 cm^{-1} in the FTIR spectra of CTF-1@400 and CTF-1@500 (Fig. 3a), along with the disappearance of the peak at 289.1 eV in the C 1s deconvoluted spectra of CTF-1@400 and CTF-1@500 (Fig. S3†), indicated the removal of carbonyl-type impurities from the triazine-based polymer during the post-treatment at high temperatures. The formation of these carbonyl-type impurities may be related to crystalliferous water (from $TsOH \cdot H_2O$) sealed and trapped within the

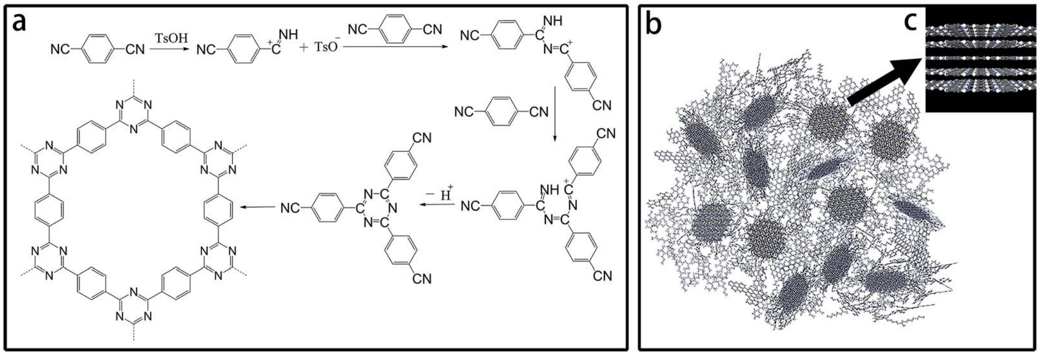

Scheme 1 (a) Trimerization reaction for DCB catalyzed by TsOH; (b) schematic for the CTF structures; and (c) schematic for crystal CTF.

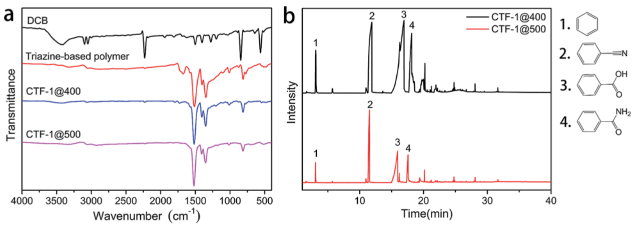

Fig. 3 (a) FTIR spectra of DCB, the triazine-based polymer, CTF-1@400 and CTF-1@500; (b) pyrogram with the fragments generated from the triazine-based polymer at 400 °C and 500 °C.

system during the first step, where hydrolysis of the nitrile groups may be triggered. Later in the second step, the high-temperature treatment of the materials in an open system facilitates the decomposition and removal of the impurities. In addition, the appearance of a new peak at 290.5 eV (related to π-carbon) in the C 1s spectrum of CTF-1@500 (Fig. S3j†) reveals the improvement of the triazine structure in larger scales. It is worth mentioning that for CTF-1@500, the peaks attributed to the nitrile groups were still detected by XPS (400.2 eV in N 1s, Fig. S3k†) and ^{13}C-solid NMR spectrum (116 ppm, Fig. S1†), which may be related to the dynamically reversible trimerization of nitriles;[34] the catalyst plays a vital role in this process. The retention of peaks centered at 168.7 eV in the deconvoluted S 2p spectra (corresponding to sulfonate structure, as shown in Fig. S3†) indicates the survival of sulfonate group at high temperatures. Table 1 shows the elemental analysis of triazine-based polymer, CTF-1@400, and CTF-1@500. It can be seen that CTF-1@500 has the C, N, and H content that is closest to the theoretical value. CTF-1@500 also has the lowest O amount, suggesting the purification of the framework by the release of oxygen-containing impurities. The similar S content in the triazine-based polymer, CTF-1@400, and CTF-1@500 indicates that the catalyst remains in the system throughout the whole process. On the other hand, the clear difference between the theoretical and experimental N content of CTF-1@500 may be attributed to the presence of residual catalyst. It has been speculated that the retention of the sulfonate structure may play a critical role in the rearrangement and development of the crystalline structure by allowing the subsequent reversible trimerization. The catalytic mechanism of the sulfonate structure will be studied in depth in our subsequent works.

Py-GC/MS experiments of the triazine-based polymer were performed at 400 and 500 °C (Fig. 3b) to study the gas evolution during the reversible trimerization reaction at high temperatures. The pyrogram fragments of benzene, cyanobenzene, benzoic acid, and benzamide confirm the decomposition and removal of the carbonyl-type impurities, as predicted from the FTIR spectra shown in Fig. 3a. Fortunately, no triazine-related fragments were found.

The abovementioned chemical characterizations revealed that as the reaction temperature increases, the orderness of framework structure is improved. PXRD was performed on the products of the two stages to reveal the trend in the crystallinity, and the patterns are shown in Fig. 4a. It can be seen that all products obtained after the two stages were partially crystalline materials, where the crystallites were distributed in a mass of amorphous triazine-based framework, as in the structure shown in Scheme 1b. The ever-strengthening diffraction peaks, especially the (100) and (001) peaks, suggested the development of lamellae with an improved stacking. The patterns were baseline corrected, smoothed, and fitted to elucidate the

Table 1 Elemental analysis of the triazine-based polymer, CTF-1@400 and CTF-1@500

	Sample	C	N	H	S	O	C/N (mol)	C/H (mol)
Theoretical	—	75	21.875	3.125	—	—	4	2
Experimental	Triazine-based polymer	69.04	15.72	3.22	3.69	8.33	5.12	1.79
	CTF-1@400	71.36	16.32	2.89	3.96	5.47	5.1	2.06
	CTF-1@500	73.99	16.37	2.92	3.82	2.9	5.27	2.11

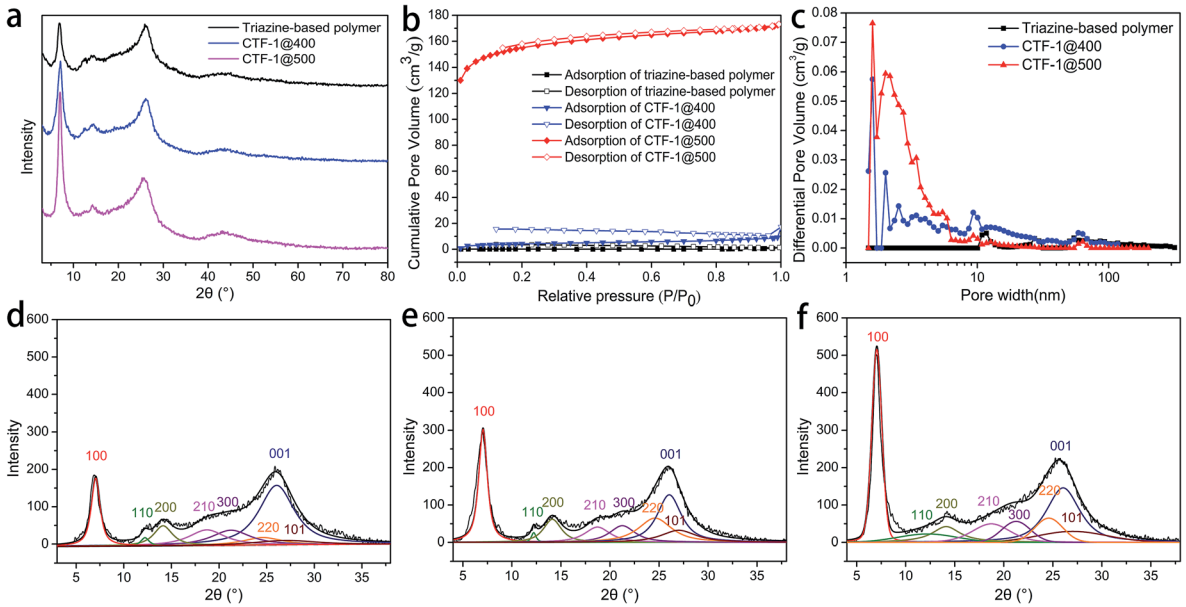

Fig. 4 (a) PXRD patterns of the triazine-based polymer, CTF-1@400 and CTF-1@500; (b) comparison of the isotherms of the triazine-based polymer, CTF-1@400 and CTF-1@500; (c) DFT pore size distribution of the triazine-based polymer, CTF-1@400 and CTF-1@500; (d) deconvoluted PXRD pattern of the triazine-based polymer; (e) deconvoluted PXRD pattern of CTF-1@400; and (f) deconvoluted PXRD pattern of CTF-1@500.

parameters for each crystal face, and the deconvoluted patterns are shown in Fig. 4d–f.[36–38] The (100) and (001) crystal faces, representing the CTF lamellae and the stacking of lamellae, respectively, were selected for the calculation. Moreover, the *d*-spacing (d_{hkl}) and the crystallite dimension (D_{hkl}) values are listed in Table 2.

During the post-treatment stage, at higher temperatures, d_{100} is closer to the theoretical value, suggesting the development of the lamellae. Based on the d_{100} value, which indicates the pore size of the framework, CTF-1@500 possesses a very pore size similar to the theoretical value. The significant increase in the D_{100} value after treatment at 500 °C implies the evident development of the lamellae. However, the D_{001} value exhibits a different trend, in which the maximum value is obtained for CTF-1@400.

The superior porosity was linked to the periodic packing of the CTF structures. Nitrogen sorption experiments at 77 K were also performed on the triazine-based polymer and CTF-1@400. Compared with CTF-1@500, the triazine-based polymer and CTF-1@400 possessed a small pore volume (Fig. 4c) and the SSAs were only 5 and 16 $m^2\ g^{-1}$, respectively. The improvement of the lamellae and their ordered packing was not accomplished before the treatment at 500 °C; thus, the intrinsic micropores enclosed by the frameworks are limited. On the other hand, for CTF-1@500, although the majority of the pores had a size within 2 nm, there were also some mesopores with a size between 2 and 6 nm, which may result from the partial decomposition of the framework. This decomposition may occur at the outer layers of the crystallites, thus resulting in a decreased D_{001}.

Conclusions

CTF-1 was prepared by a two-step route, where $TsOH \cdot H_2O$, an organic acid with medium acidity, was used as the catalyst to trigger the trimerization of DCB. Compared with the analogous framework prepared with a strong Brønsted acid such as

Table 2 Crystallite parameters of the triazine-based polymer, CTF-1@400 and CTF-1@500

	(100) crystal face				(001) crystal face			
	$2\theta_{100}$ (°)	d_{100} (Å)	β (°)	D_{100} (Å)	$2\theta_{001}$ (°)	d_{001} (Å)	β (°)	D_{001} (Å)
Theoretical	7.05	12.53[b]	—	—	26.05	3.42[b]	—	—
Triazine-based polymer	6.92[a]	12.77[c]	1.11[c]	71[c]	26.05[d]	3.42[b]	4.47[d]	18[d]
CTF-1@400	6.99[a]	12.65[c]	1.02[c]	77[c]	26.05[d]	3.42[b]	3.37[d]	24[d]
CTF-1@500	7.00[a]	12.63[c]	0.73[c]	107[c]	26.05[d]	3.42[b]	4.02[d]	20[d]

[a] Based on experimental PXRD values. [b] Theoretical values as calculated with the Materials Studio software. [c] Calculated based on the experimental θ_{100} value. [d] Calculated based on the theoretical d_{001} value.

CF_3SO_3H, CTF-1@500 prepared in this work exhibited a higher BET SSA; remarkably, this was achieved with a lower catalyst dosage. In addition, we could anticipate an enhanced performance of the CTF by incorporating more suitable monomers into our future $TsOH \cdot H_2O$-catalyzed routes.

Moreover, the evolution of the framework was studied by characterization of the chemical structure and calculation of the crystal parameters during different stages of the preparation. The results showed that the formation of the triazine-based polymer is accomplished in the presence of $TsOH \cdot H_2O$ at relatively low temperatures. In addition, the low crystallinity and porosity of the triazine-based polymer may be attributed to the presence of impurities in its structure and to a limited crystallite ordering. However, when treated at relatively high temperatures, the growth of the crystallites leads to a remarkable increase in the porosity. Finally, the method proposed in this study for evaluating the CTF crystallite size may provide a better understanding of the formation of CTFs.

Conflicts of interest

There are no conflicts to declare.

Acknowledgements

The authors would like to acknowledge Dr Yuanping Yi (Institute of the Chemistry Chinese Academy of Science) for supporting the simulations and calculations with the Materials Studio software. The authors also gratefully acknowledge the financial support of the National Natural Science Foundation of China (No. 51403218 & No. 51473171 & No. 21604090). The authors gratefully thank the Young Elite Scientist Sponsorship Program by CAST (YESS) and the Youth Innovation Promotion Association of CAS (No. 2017047).

Notes and references

1 A. Taguchi and F. Schüth, *Microporous Mesoporous Mater.*, 2005, **77**, 1–45.
2 M. Hartmann, *Chem. Mater.*, 2005, **17**, 4577–4593.
3 M. E. Davis, *Nature*, 2002, **417**, 813–821.
4 Y. Zhao, K. X. Yao, B. Teng, T. Zhang and Y. Han, *Energy Environ. Sci.*, 2013, **6**, 3684.
5 S. Hug, M. B. Mesch, H. Oh, N. Popp, M. Hirscher, J. Senker and B. V. Lotsch, *J. Mater. Chem. A*, 2014, **2**, 5928–5936.
6 H. Liao, H. Ding, B. Li, X. Ai and C. Wang, *J. Mater. Chem. A*, 2014, **2**, 8854.
7 J. Lee, O. K. Farha, J. Roberts, K. A. Scheidt, S. T. Nguyen and J. T. Hupp, *Chem. Soc. Rev.*, 2009, **38**, 1450–1459.
8 J. R. Li, R. J. Kuppler and H. C. Zhou, *Chem. Soc. Rev.*, 2009, **38**, 1477–1504.
9 A. I. Cooper, *CrystEngComm*, 2013, **15**, 1483.
10 B. P. Biswal, S. Kandambeth, S. Chandra, D. B. Shinde, S. Bera, S. Karak, B. Garai, U. K. Kharul and R. Banerjee, *J. Mater. Chem. A*, 2015, **3**, 23664–23669.
11 L. Bai, Q. Gao and Y. Zhao, *J. Mater. Chem. A*, 2016, **4**, 14106–14110.
12 P. Puthiaraj, Y.-R. Lee, S. Zhang and W.-S. Ahn, *J. Mater. Chem. A*, 2016, **4**, 16288–16311.
13 R. K. Yadav, A. Kumar, N.-J. Park, K.-J. Kong and J.-O. Baeg, *J. Mater. Chem. A*, 2016, **4**, 9413–9418.
14 X. Ding, L. Chen, Y. Honsho, X. Feng, O. Saengsawang, J. Guo, A. Saeki, S. Seki, S. Irle, S. Nagase, V. Parasuk and D. Jiang, *J. Am. Chem. Soc.*, 2011, **133**, 14510–14513.
15 Q. Fang, J. Wang, S. Gu, R. B. Kaspar, Z. Zhuang, J. Zheng, H. Guo, S. Qiu and Y. Yan, *J. Am. Chem. Soc.*, 2015, **137**, 8352–8355.
16 S. Dalapati, E. Jin, M. Addicoat, T. Heine and D. Jiang, *J. Am. Chem. Soc.*, 2016, **138**, 5797–5800.
17 L. Stegbauer, K. Schwinghammer and B. V. Lotsch, *Chem. Sci.*, 2014, **5**, 2789–2793.
18 S. Lin, C. S. Diercks, Y. B. Zhang, N. Kornienko, E. M. Nichols, Y. Zhao, A. R. Paris, D. Kim, P. Yang, O. M. Yaghi and C. J. Chang, *Science*, 2015, **349**, 1208–1213.
19 H. Xu, J. Gao and D. Jiang, *Nat. Chem.*, 2015, **7**, 905–912.
20 H. Xu, S. Tao and D. Jiang, *Nat. Mater.*, 2016, **15**, 722–726.
21 A. P. Cote, A. I. Benin, N. W. Ockwig, M. O'Keeffe, A. J. Matzger and O. M. Yaghi, *Science*, 2005, **310**, 1166–1170.
22 S. Y. Ding and W. Wang, *Chem. Soc. Rev.*, 2013, **42**, 548–568.
23 P. Kuhn, M. Antonietti and A. Thomas, *Angew. Chem., Int. Ed. Engl.*, 2008, **47**, 3450–3453.
24 J. Liu, E. Zong, H. Fu, S. Zheng, Z. Xu and D. Zhu, *J. Colloid Interface Sci.*, 2012, **372**, 99–107.
25 A. Bhunia, I. Boldog, A. Möller and C. Janiak, *J. Mater. Chem. A*, 2013, **1**, 14990.
26 F. Chang, J. Guo, G. Wu, L. Liu, M. Zhang, T. He, P. Wang, P. Yu and P. Chen, *RSC Adv.*, 2015, **5**, 3605–3610.
27 W. Suksaengrat and P. Srepusharawoot, *Microelectron. Eng.*, 2013, **108**, 192–194.
28 P. Katekomol, J. Roeser, M. Bojdys, J. Weber and A. Thomas, *Chem. Mater.*, 2013, **25**, 1542–1548.
29 J. Liu, Y. Hu and J. Cao, *Catal. Commun.*, 2015, **66**, 91–94.
30 P. Kuhn, A. Thomas and M. Antonietti, *Macromolecules*, 2009, **42**, 319–326.
31 P. Kuhn, A. Forget, D. Su, A. Thomas and M. Antonietti, *J. Am. Chem. Soc.*, 2008, **130**, 13333–13337.
32 X. Zhu, C. Tian, S. M. Mahurin, S. H. Chai, C. Wang, S. Brown, G. M. Veith, H. Luo, H. Liu and S. Dai, *J. Am. Chem. Soc.*, 2012, **134**, 10478–10484.
33 C. Reece, D. J. Willock and A. Trewin, *Phys. Chem. Chem. Phys.*, 2015, **17**, 817–823.
34 S. Ren, M. J. Bojdys, R. Dawson, A. Laybourn, Y. Z. Khimyak, D. J. Adams and A. I. Cooper, *Adv. Mater.*, 2012, **24**, 2357–2361.
35 J. I. Langford and A. J. C. Wilson, *J. Appl. Crystallogr.*, 1978, **11**, 102–113.
36 J. M. Jiménez Mateos, E. Romero and C. G. De Salazar, *Carbon*, 1993, **31**, 1159–1178.
37 H. H. Chang, L. K. Chang, C. D. Yang, D. J. Lin and L. P. Cheng, *J. Membr. Sci.*, 2016, **513**, 186–196.
38 R. M. Mohanty, K. Balasubramanian and S. K. Seshadri, *J. Alloys Compd.*, 2007, **441**, 85–93.